CCFE
CULHAM CENTRE FOR FUSION ENERGY

UK Atomic Energy Authority

UKAEA-CCFE-CP(20)74

Anna Widdowson, J.P. Coad, E. Alves, A. Baron-Wiechec, N.P. Barradas, N. Catarino, V. Corregidor, K. Heinola, S. Krat, M. Mayer, K. Mizohata, M. Sertoli, JET contributors

Deposition of metallic impurities in JET ITER-like wall

Deposition of metallic impurities in JET ITER-like wall

Anna Widdowson, J.P. Coad, E. Alves, A. Baron-Wiechec, N.P. Barradas, N. Catarino, V. Corregidor, K. Heinola, S. Krat, M. Mayer, K. Mizohata, M. Sertoli, JET contributors

This paper has been submitted to
23rd International Conference on Plasma Surface Interactions in Controlled Fusion Devices (PSI), Princeton, NJ, USA, 17-22 June 2018

Deposition of impurity metals during campaigns with the JET ITER-like Wall

A Widdowson[a*], JP Coad[a], E Alves[b], A Baron-Wiechec[a], N Catarino[b], V Corregidor[b], K Heinola[c,d], S Krat[e], C Makepeace[f,a], GF Matthews[a], M Mayer[g], K Mizohata[d], M Sertoli[g] and JET Contributors[†]

EUROfusion Consortium, JET, Culham Science Centre, Abingdon, OX14 3DB, UK

[a]*Culham Centre for Fusion Energy, Culham Science Centre, Abingdon, OX14 3DB, UK*

[b]*Instituto Superior Técnico, Universidade de Lisboa, 1049-001 Lisboa, Portugal*

[c]*International Atomic Energy Agency, Vienna International Centre, PO Box 100, 1400 Vienna, Austria*

[d]*University of Helsinki, P.O. Box 64, 00560 Helsinki, Finland*

[e]*National Research Nuclear University MEPhI, Moscow, Russia*

[f]*Department of Materials, University of Oxford, Parks Road, Oxford OX1 3PH, UK*

[g]*Max-Planck-Institut für Plasmaphysik, 85748 Garching, Germany*

[†] *See the author list of X. Litaudon et al 2017 Nucl. Fusion 57 102001*

Abstract

Post mortem analysis shows that mid and high atomic number metallic impurities are present in deposits on JET plasma facing components with the highest amount of Ni and W, and therefore the largest sink, being found at the top of the inner divertor. Sources are defined as "continuous" or "specific", in that "continuous" sources arise from ongoing erosion from plasma facing surfaces and "specific" are linked with specific events which decrease over time until they no longer act as a source. This contribution evaluates the sinks and estimates sources, and the balance gives an indication of the dominating processes. Charge exchange neutral erosion is found to be the main source of nickel, whereas erosion of divertor plasma

facing components is the main source of tungsten. Specific sources are shown to have little influence over the global mid- and high-Z impurity concentrations in deposits.

PACS: 52.40.Hf, 52.55.Fa,

PSI-20 keywords: JET, Erosion, Deposition, Impurities, Nickel, Tungsten

**Corresponding author address:* Culham Science Centre, Abingdon, OX14 3DB, UK

**Corresponding author E-mail:* anna.widdowson@ukaea.uk

1. Introduction

After three operating campaigns of JET with the ITER-like Wall (JET-ILW) the evolving picture of fuel retention and material migration has been well documented [1] [2] [3] [4] [5] [6] [7] [8] [9] [10] [11][12][13]. The effect of the campaign average plasma configurations on the global erosion of plasma facing components (PFCs), migration of eroded material and eventual deposition are largely understood. Erosion from plasma interaction may occur as a result of several processes; (i) during limiter plasmas - erosion of limiters where direct contact between plasma and PFCs occurs, (ii) during divertor plasmas - erosion of divertor surfaces due to sputtering by incoming energetic ions at or near the strike point positions, and (iii) for all phases - charge exchange neutrals (CXN) coming from the plasma that can erode all surfaces, including those that are recessed from the plasma, i.e., that do not experience direct plasma contact. The erosion processes (i) and (iii) occur in the main chamber and provide a source of impurities which can enter the plasma or the scrape off layer (SOL). Impurities in the SOL migrate around the edge of the plasma primarily to the inner divertor surfaces during divertor plasmas giving rise to deposition. Most deposition occurs at the upper inner divertor as this is accessible from the SOL for all plasma configurations, however more complicated patterns of deposition arise due to variations in the location of the

strike point positions. Deposition can also occur in the main chamber mainly during limiter plasmas, for example at the ends of limiter tiles are located deep into the SOL. For JET the main deposition impurities are beryllium (Be) eroded from the main chamber limiters, carbon (C) a residual in the machine coming from remote components, and oxygen (O) due to a low-level air leak. Deuterium (D) is the principle plasma fuel some of which is co-deposited with the Be and C. Mid-atomic number (Z) and high-Z metals are also found in deposits. The presence of tungsten (W) and molybdenum (Mo) in deposits is not surprising as all divertor PFCs and some recessed main chamber PFCs have a W surface, either as bulk material or as a coating on a carbon fibre composite (CFC) substrate with a Mo interlayer and W top layer. Mid-Z impurities such as nickel (Ni), chromium (Cr) and iron (Fe) are also abundant in JET as the vessel's structural components are made of nickel alloys such as Inconel.

The presence of mid- and high-Z metallic impurities affect plasma operations, cooling the plasma through energy absorption leading to radiation losses. The concentrations of mid- and high-Z impurities in deposits will be related to their plasma concentrations. This manuscript reports the mid- and high-Z impurities found in JET PFCs and the magnitudes of the potential sources are discussed.

2. Experimental Details

After each JET operating period a set of PFCs (tiles) and other components are removed for analysis to understand surface erosion, deposition and fuel retention. JET-ILW has now completed three periods of operation; 2011-12 (ILW1), 2013-14 (ILW2) and 2015-16 (ILW3) and analysis of tiles allows comparison between these periods. This manuscript does not provide the details of erosion and deposition of the major Be impurity and co-deposition of D, C and O; it reports primarily on W, Ni, Cr and Fe impurities. Details of Be, D, C, O analysis can be found elsewhere along with details of the analytical methods used [1] [2] [3] [4] [5] [6] [7] [8] [9] [10] [11][12][13]. The overall concentrations of the minor mid-

and high-Z impurities follow the deposition patterns of Be, D, C, O. In the following sections the results presented on W divertor tiles are mainly for Ni, Cr, Fe due to the difficulty in accurately determining W in deposits on a W substrate. For the Be main chamber tiles the results presented are mainly W, as Ni analysis is not possible for ILW1 and ILW2 vintage tiles as they were marker tiles designed to measure erosion/deposition by coating with an interlayer of Ni (~3 μm) and a top coat (~7 μm) of Be: tiles exposed during ILW3 did not have the marker coatings. Results for diagnostics located in the divertor corners are for W as the substrate was either steel (grade with no W) or Ni-based alloys.

3. Results and discussion

3.1 Mid- and high-atomic number metal impurities in the divertor

3.1.1 Mid-atomic number impurities

Beryllium eroded from the main chamber has been shown previously to be mostly deposited at the top of the inner divertor on Tile 1 and the High Field Gap Closure (HFGC) tile [1][5][14][15]. The deposition on Tile 1 was restricted to the upper part of the tile during ILW1 (s-coordinate 162-280 mm – see inset in Figure 1) but extended over the rest of the tile for ILW2 due to the use of a wider range of strike point positions [16]. Figure 1 shows that the situation is the same for Ni, and the profile for ILW3 is similar to that for ILW2: the tiles analysed were each exposed for just the one ILW campaign. The amounts of Ni averaged over Tile 1 for ILW1, 2 and 3 are 1.4, 1.8 and 2.4% of the corresponding amounts of Be (respectively). The Cr and Fe concentrations follow the same pattern as the Ni but are each smaller by a factor 3-4. This agrees with the relative concentrations in Inconel (Ni 50-80%, Cr ~20%, Fe 5-20% depending on grade) and points to Inconel as the source of these impurities (see also section 3.3.). Extrapolating the Ni deposition at the upper inner divertor Tile 1 for

the whole divertor gives a total deposition of the order 10^{22} Ni atoms for a campaign consisting of ~ 5 x 10^4 s of plasma.

As for Tile 1, mid-Z impurities are found in all deposits in the divertor. For example, the re-deposition bands on inner divertor corner Tile 4 and outer divertor corner Tile 6 [3][15][11][16] also contain Ni, Cr and Fe. For Tile 6 the amount of deposition increases significantly in this deposition band from 1 ×10^{18} Be at/cm^2 to 1 ×10^{19} Be at/cm^2 for ILW1 and ILW2 respectively. The overall increase in deposition could partly be due to increased time for the outer strike point (OSP) on Tile 6 of 2.8 x 10^4 s in ILW2 compared with 1.0 x 10^4 s in ILW1 [11], however, the amount of Ni after ILW3 remains similar to ILW2 even though the OSP on Tile 6 increases again to 4.4 x 10^4 s, suggesting a decrease in Ni concentration with respect to Be deposition (although the full analysis for Be deposition is still to be confirmed). After ILW2 the concentration of Ni in the Tile 6 deposition band was 10% of the Be concentration, whereas at the inner divertor corner Tile 4 the Ni concentration was 1 ×10^{17} at/cm^2, only 1-2 % of the Be concentration, which is similar to Tile 1. The reason for the differences in Ni concentrations at the inner and outer divertor and the peak in Ni concentration on Tile 6 following ILW2 operations may be due to the melting of three tile tie rods at the outer divertor which occurred during ILW2 providing an additional source of Ni, Cr and Fe. This is discussed further in section 3.3.

Moon et al [17] compared deposits on molybdenum mirror samples exposed to ILW3 with those exposed for the three campaigns (ILW1-3). In general, impurity concentrations were about three times greater following the three campaigns than after just ILW3, and the outer divertor values were 2-5 times greater than those from the inner corner, for equivalent positions. However, Ni levels following ILW3 did appear to be rather closer to the ILW1-3 level than they are elsewhere.

3.1.2 W impurities in the divertor

All the PFC surfaces in the divertor are W - either as bulk W (Tile 5) or as thick W coatings (all other PFCs). On all these surfaces it is not possible to prove unambiguously whether W seen in surface analysis IBA spectra is deposition or from the W substrate. However, there are a number of diagnostics at the divertor corners shadowed from direct plasma bombardment that are not made from W such as louvre clips, mirrors, rotating collectors and Quartz Microbalances [18] on which W deposition can be measured. As an example, Figure 2 shows W analysis data from a louvre clip at the outer divertor corner exposed to ILW2. The W level is in the range 2-10% of the Be concentration on the clip, which is typical for the many diagnostic components analysed (including those reported in [17][19]), and suggests that the total W deposition in the divertor corners during one ILW campaign is in the range 10^{20} to 10^{21} atoms. However, it should be borne in mind that the majority of the (Be) deposition occurs at the top of the inner divertor, including 10^{20} at/cm^2 Be over a poloidal distance of >10 cm [3]. This equates to ~10^{24} Be atoms toroidally, and if W is at 2% (similar to Ni) throughout these deposits then ~2×10^{22} atoms W would be included. The remote location of the louvre clip may indicate that migration of W is by line of sight transport due to erosion of W coatings when the strike point is on Tile 6 [20][21]. However, the end of the louvre clip blade has no direct line of sight from Tile 6, therefore migration must be multi-step which could involve; (i) reflections, i.e., low sticking coefficient, (ii) erosion of deposited W by sufficiently high energy neutrals for sputtering, (iii) high sputtering yield of W deposits or (iv) transport of W via formation of volatiles, e.g., oxides. Further modelling is required to understand the relative impact of these processes.

3.2 Mid- and high-atomic number metal impurities in the main chamber

3.2.1 Mid-atomic number impurities

The inner wall of the JET vessel has 16 poloidal Inner Wall Guard Limiter beams (IWGL), each of which is 320 mm wide; of these ten are made of bulk Be, and the others are either W-coated CFC or Be-coated Inconel and are recessed at least 25 mm behind the Be limiters. The gaps between the limiters are covered with either Be-coated Inconel tiles (69%) or W-coated CFC tiles (31%) recessed 40 mm behind the Be limiters; a schematic diagram is shown in [8].

Ni, Cr and Fe will have deposited on the Be limiter surfaces, however whilst analysis of Ni cannot be determined unambiguosly for ILW1 and ILW2 due to marker coatings (see section 2), data for ILW3 is available. Figure 3 (a) shows the Ni, Cr and Fe concentrations across an IWGL Be limiter from the mid-plane that was exposed just during ILW3. The plasma is in contact with the central region of this tile during the limiter phases of each discharge (i.e. ramp-up and ramp-down), and the area is one of net erosion (by up to 60 μm during ILW1 [12]). Towards the toroidal ends of the limiter, the surfaces are progressively deeper into the SOL due to the curvature of the tile, and the region changes from net erosion to net deposition. The very ends of the tiles are shadowed by the next limiter in the poloidal direction, so the deposition there is reduced. The distribution of metals on the mid-plane IWGL reflects this description; their concentration is low in the central region of the tile and peaked towards the ends. Cr and Fe are also seen along with W in cross section transmission electron micrographs of deposits on Be limiter tiles from ILW1, an example for Cr is also shown in Figure 3 (b). Figure 3 (a) clearly indicates that the relative concentrations of Ni, Cr and Fe in the deposit are the same as for Inconel alloys.

3.2.2 W impurities in the main chamber

Figure 4 shows the W concentrations found on IWGL tiles exposed at the same mid-plane position for each of the ILW campaigns. As for Ni, Cr and Fe the W levels are low in the eroded central region. For ILW2 and ILW3 the W concentration decreases at the very ends of the tile (+/- 160mm) due to the shadowing by the next limiter, however for ILW1 it increases to the very ends. This is likely due to an additional source of W in the main chamber during ILW1 which is discussed in section 3.3.

Limiter tiles from the top and near the bottom of the limiter were also analysed after each ILW campaign. These tiles do not show erosion in their central region because in general limiter plasmas, which have a small radius compared with the limiter curvature, are not in direct contact with the ends of the limiter beams for any significant time. Nor do the top and bottom tiles show such clear W peaks at the edges of the tiles after ILW1. They do show the classic IWGL pattern of deposition on the right-hand side towards the top, and to the left-hand side towards the bottom of the limiter (see, for example [22] for the JET-carbon phases).

There are also Be limiters protecting the outer wall and the many diagnostics and heating systems located there. Selected tiles from one of the Be Wide Poloidal Limiters (WPL) are also analysed after exposure to each campaign, these comprise seven tile segments toroidally as seen in Figure 5. The W deposition on the mid-plane tile is also classic in behaviour with erosion of a few microns in the central region (for ~100 mm either side of the tangency point for limiter discharges) and deposition peaking deeper into the SOL, as shown in Figure 5. Figure 5 does show one anomaly from this pattern: there is increased deposition to the right-hand side of the central tile exposed to ILW1 with a cut-off at the edge of this piece at the toroidal position on the tile = 60 mm; there is probably a larger misalignment between the central Be segment and the piece to its right creating a larger shadowed area on

the right-hand side of the central segment where material is deposited. Extrapolating for IWGL and WPL tiles the deposition of W on limiter tiles is ~ 10^{21} atoms for a campaign.

Figure 3 and Figure 4 show that Ni concentrations are a factor 2-3 times higher than for W on the mid-plane IWGL, which indicates a higher source for Ni than W reaching the main chamber. The analysis of the W and Ni sources potentially reaching the main chamber are discussed in section 3.3 and are a similar order of magnitude. It is not possible to determine the concentration relative to Be from IBA data due to the Be substrate.

3.3 Sources of mid- and high-atomic number impurities

There are two categories of sources of mid-Z and high-Z impurities to consider; sources that are on-going during plasma operations "continuous sources", and sources that exist for a limited time "specific sources". In both cases the impurities migrate through multi-step erosion/deposition processes until they reach a surface where they can no longer be re-eroded. A continuous source however will result in a continual build-up of impurities on remote surfaces whereas a specific source will decrease with time. In this section examples of continuous and specific sources for both mid- and high-Z impurities are presented and where possible their relative magnitude evaluated.

3.3.1 Continuous sources

All divertor PFCs and some recessed main chamber PFCs have a W surface, either as bulk material or as a coating on a CFC substrate with a Mo interlayer and W top layer, therefore there is a significant source of W due to sputtering at these surfaces. W erosion is dominated by sputtering at the strike point on divertor PFCs, but other contributions include CXN erosion of W coated surfaces at the inner wall and field line connections to divertor PFCs during ICRF heating [23], these latter two mechanisms and potential sources are discussed later in this section. W erosion of divertor PFCs is measured as ~ 1.5 μm (~10^{19}

at/cm^2) for ILW2 on Tile 5 and Tile 6 where the strike point was located [14]. Taking a conservative total erosion area of 10.8 x 10^3 cm^2, i.e., two regions extending 5 cm poloidally on Tile 5 and Tile 6 for ILW2 (see [14]) and including shadowing between tiles, this constitutes a potential net W source up to 10^{23} atoms which is considerably higher than the amount of 10^{20} - 10^{21} atoms which is found to migrate to the remote corners. However, as mentioned in section 3.2.2, if W is ~2% on the deposited Be elsewhere in the divertor, ~2 × 10^{22} W atoms may be in deposits at the top of the inner divertor. Furthermore, some of the eroded W will be deposited locally either within the gaps between lamellae of Tile 5 or in the deposition peak at the bottom of the sloping part of Tile 6. Nevertheless, not all of the eroded material has been accounted for in the *post mortem* analysis of the divertor deposits and it would appear that a large fraction of the W eroded from Tile 5 and 6 must enter the plasma in order to migrate to the main chamber in addition to Tile 1 and the HFGC tile.

The JET vessel is manufactured mainly from Inconel® 600, and support brackets, fastenings and in-vessel furniture are also made from Inconel, or similar Ni-based alloys. Therefore, despite all surfaces with direct interaction with the confined plasma and all the inner wall PFCs being made of either Be or W, 85.4 m^2, > 60 % of the main chamber surface at the top and outer vessel walls is unclad Inconel and is exposed to CXNs exiting the plasma. CXNs can have sufficient energy to sputter elements from these surfaces (mostly Ni, Cr and Fe), and this is assumed to be the reason why these elements have always been observed in the JET plasma, probably after two (or more) step processes via limiter surfaces, and also found in deposits on PFCs [22].

Indeed erosion of the recessed surfaces of the JET vessel wall by CXNs has been measured throughout JET operations using C, Be and W coatings on samples inserted into inner wall cladding tiles [8][24]. The most recently analysis for JET-ILW shows erosion rates of 0.6 × 10^{14} at/cm^{2}s and 9.2 × 10^{11} at/cm^{2}s for Be and W respectively [8]. Assuming mono-

energetic CXN, the energy that is compatible with these two values is 635eV, and would give a yield for Ni of 3.7 x 10^{13} at/cm^{2}s [25][26]; a more detailed calculation using a Maxwellian CXN energy distribution might give a slightly different Ni erosion rate, but the resulting Ni source is likely to be in the range 10^{23} – 10^{24} atoms during a campaign lasting of the order 5 $\times 10^4$ s. Even if parts of the vacuum vessel are coated with impurities (e.g. C, Be) from previous operations, these figures suggest that CXN erosion may be the largest, and a sufficient, source of mid-Z impurities in the main chamber.

An increase in mid- and high-Z impurities in the plasma is observed with ICRF operation where field line connections with divertor and main chamber PFCs will result in some erosion. Wetted areas include the top of the inner divertor and outer divertor [23]. The top of the outer divertor is a net erosion zone and can be a source of W, and erosion of just 0.01 - 0.1 μm of W could provide a source of 10^{21} - 10^{22} W atoms over a campaign. At the top of the inner divertor (Tile 1 and High Field Gap Closure tiles further inboard) the PFCs are covered by Be deposits containing, amongst other impurities, Ni at a concentration of 10^{18} at/cm^2 and although not directly quantified for Tile 1, W is likely to be at a similar level. At these surfaces any erosion will be of the deposits (and not pure W) resulting in a lesser Ni (and W) source of 10^{21} atoms within ~ 10^{23} atoms Be per campaign if ~ 10% of the deposits were eroded during ICRH. Other field line connections to the inner and outer main chamber wall may also re-erode deposits which have formed on limiters. In this respect these interactions may serve to re-erode mid- and high-Z impurities from other sources. The ICRF antenna itself could also act as a source of Ni. Whilst much of the antennae is surrounded by Be tiles and components, there remain some Inconel components “knuckles” which could increase the Ni source. However this source does not need to be invoked to balance the Ni sources and sinks: CXN erosion in the main chamber from 10% of the unclad Inconel vessel wall (10^{22}-10^{23} as discussed in section 3.3.1) can already provide for the divertor deposition

sink of 10^{22} Ni atoms (as discussed in section 3.2.1). Nevertheless, a further spectroscopic study of the levels of Ni in the plasma may assist in confirming which sources are significant.

3.3.2 Specific sources

A source of mid-Z impurities in the JET plasma was suspected to be due to the failure of three tile tie rods during ILW2. Tie rods made of Inconel® 718 are inserted into the CFC substrate of divertor tiles to prevent tiles from breaking apart in the event of cracking between fibre planes. When the vessel was vented and an in vessel photographic survey undertaken, three broken tie rods which were mounted in a vertical position in Tile position 7 were found partially melted in the outer divertor gap leading to the pumps; the three locations were in octants 1, 6 and 7. With melting having occurred during *outer corner* plasma configurations, i.e., OSP on Tile 6, it was thought that this could be a source of mid-Z impurities in the plasma, and it might be concluded that the dramatic increase in Ni concentration in the deposition band Tile 6 from ILW1 to ILW2 (see section 3.1) is indicative of this, but this is not necessarily the case as the difference in OSP time on Tile 6 for ILW1 and ILW2 has a significant influence on the total amount of deposit (including Ni). Instead a comparison of the Ni concentration with respect to Be in deposits should be made. For ILW2 the Ni concentration in the deposition band on Tile 6 was 10% of Be and for Tile 4 was 2% (similar for Tile 1 see section 3.1). As impurities in deposits built up primarily due to material migration from the SOL it follows that impurity concentrations in deposits might reflect plasma concentrations, therefore the higher concentration of Ni on Tile 6 is an anomaly and may be due to the tie rod melting. Initial results for ILW3 suggest that the concentration of Ni with respect to Be has deceased, which would be consistent with the Ni source liberated by the tie rod melting in ILW2 having already migrated to remote regions before ILW3. In fact many Tile 6s were replaced between ILW2 and ILW3.

There is no conclusive evidence that the tie rod melting resulted in an increase in Ni in the plasma beyond the outer divertor corner. There are no anomalous deposits of Ni from post-mortem analyses, and so far analysis of the VUV spectroscopy of Ni, Cr or Fe cannot be linked consistently with any specific period when each tie rod may have failed and started to melt (or a general increase once melting was ongoing) with *outer corner* plasma configurations.

Another metric for analysis of impurities is to consider transient impurity events (TIE), i.e., excursions in optical spectroscopy signals due to particles entering the plasma. The number of TIEs for W and Ni/Cr/Fe are plotted for characteristic spectral lines for each category against the pulse number during each campaign, as described in [27] and shown in Figure 6. It is clear that there is a steady decline in the average number of events from ILW1 to ILW2 to ILW3. There is also a peak in the early discharges for the ILW1 and ILW2 campaigns, which may result from dust and debris caused by in-vessel work and installation of new components during the preceding shut-down. For example, W particles could be ejected during plasma operation from coating asperities and imperfections on new tiles installed for ILW1, or Ni, Cr, Fe debris could remain in vessel after installation work involving cutting, welding and grinding at the vessel wall after ILW1 and ILW2 which would decrease over time. Notably, no significant increase in TIE for Ni, Cr, Fe was observed during ILW2 that might be correlated with the tie rod failures mentioned above, as might be expected if molten material was ejected from this location.

Many of the W transients observed may be ascribed to small particles of W coating entering the plasma and such particles have been observed by infrared camera viewing systems being ejected from the divertor region. In addition small W particles were observed by TEM in deposits following ILW1 [28].

W coatings were also found to undergo cracking and delamination due to expansion mis-match in one direction between the coating and substrate as a result of rapid thermal cycling due to plasma interaction (which can be between 200° and 1000°C). This was particularly evident for divertor Tile 6s and Tile7s during ILW1 and ILW2 where some tiles were prone to coating failure due to a process issue for a specific coating batch: these tiles were replaced between ILW2 and ILW3. Analysis of W TIEs suggests that the source is 10^{21} W atoms [27] whereas an estimate of cracking/delamination area from divertor PFCs could yield up to 10^{23} W atoms. This suggests that only a small percentage of particles travel to the plasma. There is evidence from scanning electron microscopy that suggests thermal cracking of coatings is associated with melting and formation of small spheres alongside the cracks rather than ejection of particles. In addition tungsten particles encapsulated by deposits have been observed [11]. The analysis also shows that overall TIEs constitute a specific source decreasing with operating time which is inconsistent with our understanding of time evolution of W coating cracking issues in JET.

In the shutdown after ILW1 the W coating on some tiles alongside the channel for the neutral beam entering the vessel from the mid-plane of Octant 8 and Octant 4 were found to have been eroded [12]. The area of coating eroded was ~100 cm^2, which equates to 10^{22} W atoms; there does not appear to have been significant further erosion during ILW2 and 3. This W may have contributed to the general level of W deposition during ILW1 and constitutes a specific source and may explain the increased level of W on the ends of the ILW1 mid-plane IWGL (Figure 4). Some of the TIE may well have been triggered by this coating erosion.

4. Conclusions

The sources and sinks for mid- and high-Z impurities found from *post mortem* analysis help to ascertain the erosion processes dominating their production. Although the Ni concentration on the IWGL for ILW3 is slightly higher than the W concentration, they are

essentially of the same order of magnitude, thus indicating that the sources are of similar magnitude. The main candidate for Ni is the CXN erosion of the recessed main vessel chamber and is potentially of the order $10^{23} – 10^{24}$ atoms per campaign; however, much of the vessel wall is coated with impurities which somewhat reduces the source potentially by up to 90%. For W there are three possible main sources; (i) erosion from the outer divertor at 10^{23} atoms per campaign, (ii) erosion due to field line connections at the top of the outer divertor, which could provide 10^{21} - 10^{22} atoms for 0.01 - 0.1 μm net erosion and (iii) coating imperfections and fatigue cracking.

Overall, specific sources do not have a significant bearing as they decrease over time and eventually the source material migrates to deposits on remote surfaces. The melted tie rods were perceived as affecting plasma operations, but the increase in Ni concentration on Tile 6 shown in *post mortem* analysis is probably only a local effect as no consistent correlation with Ni concentration in the plasma from VUV and TIE measurements has been established with *outer corner* plasma configurations.

The main sink for impurities is the top of Tile 1 at the inner divertor, where the most deposition and fuel retention occurs. The sink is estimated at 10^{22} Ni atoms (and although not quantified by IBA is probably of a similar magnitude for W) per campaign. In terms of mid- and high-Z material balance this is fairly consistent with the dominant source mechanisms identified which range from $10^{22} – 10^{23}$ atoms for Ni and W. The comparison of the Ni sources and sinks indicates that there is no need to invoke a source originating from the ICRH antennae to achieve a material balance.

The presentation of the mid- and high-Z impurities has highlighted some areas for further work including; further spectroscopic evaluation of Ni and W sources in the plasma to compare with the sources ascertained from material balance, modelling and measurement of CXN neutral erosion of the vessel wall for material lifetime studies of future fusion devices

and the continued reporting of W and Ni, Cr, Fe data from *post mortem* analysis, an area which has primarily concentrated on analysis of D, Be, C and O, in order to continue to detail the material balance.

5. Acknowledgements

This work has been carried out within the framework of the EUROfusion Consortium and has received funding from the Euratom research and training programme 2014-2018 under grant agreement No 633053 and from the RCUK Energy Programme [grant number EP/I501045]. To obtain further information on the data and models underlying this paper please contact PublicationsManager@ccfe.ac.uk. The views and opinions expressed herein do not necessarily reflect those of the European Commission.

6. References

[1] K. Heinola, A. Widdowson, J. Likonen, E. Alves, A. Baron-Wiechec, N. Barradas, S. Brezinsek, N. Catarino, P. Coad, S. Koivuranta, G.F. Matthews, M. Mayer, P. Petersson, JET-EFDA Contributors, Fuel retention in JET ITER-Like Wall from post-mortem analysis, J. Nucl. Mater. 463 (2015) 961–965. doi:10.1016/j.jnucmat.2014.12.098.

[2] K. Heinola, J. Likonen, T. Ahlgren, S. Brezinsek, G. De Temmerman, I. Jepu, G.F. Matthews, R.A. Pitts, A. Widdowson, Long-term fuel retention and release in JET ITER-Like Wall at ITER-relevant baking temperatures, Nucl. Fusion. 57 (2017) 086024. doi:10.1088/1741-4326/aa747e.

[3] K. Heinola, A. Widdowson, J. Likonen, T. Ahlgren, E. Alves, C.F. Ayres, A. Baron-Wiechec, N. Barradas, S. Brezinsek, N. Catarino, P. Coad, C. Guillemaut, I. Jepu, S. Krat, A. Lahtinen, G.F. Matthews, M. Mayer, JET Contributors, Experience on divertor fuel retention after two ITER-Like Wall campaigns, Phys. Scr. T170 (2017) 014063. doi:http://iopscience.iop.org/article/10.1088/1402-4896/aa9283/meta.

[4] N. Catarino, A. Widdowson, A. Baron-Wiechec, J.P. Coad, K. Heinola, M. Rubel, E. Alves, JET Contributors, Time-resolved deposition in the remote region of the JET-ILW divertor: measurements and modelling, Phys. Scr. T170 (2017) 014059. http://iopscience.iop.org/article/10.1088/1402-4896/aa8c9a/pdf.

[5] M. Mayer, S. Krat, W. Van Renterghem, A. Baron-Wiechec, S. Brezinsek, I. Bykov, P. Coad, Y. Gasparyan, K. Heinola, J. Likonen, A. Pisarev, C. Ruset, G. de Saint-Aubin, A. Widdowson, JET Contributors, Erosion and deposition in the JET divertor during the first ILW campaign, Phys. Scr. T167 (2016) 014051. doi:10.1088/0031-8949/T167/1/014051.

[6] P. Petersson, M. Rubel, H.G. Esser, J. Likonen, S. Koivuranta, A. Widdowson, Co-

deposited layers in the divertor region of JET-ILW, J. Nucl. Mater. 463 (2015) 814–817. doi:10.1016/j.jnucmat.2014.12.077.

[7] S. Koivuranta, J. Likonen, A. Hakola, J.P. Coad, A. Widdowson, D.E. Hole, M. Rubel, JET-EFDA Contributors, Post-mortem measurements of fuel retention at JET, Phys. Scr. T159 (2014) 014052. doi:10.1088/0031-8949/2014/T159/014052.

[8] S. Krat, Y. Gasparyan, A. Pisarev, I. Bykov, M. Mayer, G. de Saint Aubin, M. Balden, C.P. Lungu, A. Widdowson, JET-EFDA contributors, Erosion at the inner wall of JET during the discharge campaign 2011–2012 in comparison with previous campaigns, J. Nucl. Mater. 456 (2015) 106–110. doi:10.1016/j.jnucmat.2014.08.010.

[9] J. Likonen, K. Heinola, A. De Backer, S. Koivuranta, A. Hakola, C.F. Ayres, A. Baron-Wiechec, P. Coad, G.F. Matthews, M. Mayer, A. Widdowson, JET Contributors, Deuterium trapping and release in JET ITER-like wall divertor tiles, Phys. Scr. T167 (2016) 014074. doi:10.1088/0031-8949/T167/1/014074.

[10] A. Baron-Wiechec, A. Widdowson, E. Alves, C.F. Ayres, N.P. Barradas, S. Brezinsek, J.P. Coad, N. Catarino, K. Heinola, J. Likonen, G.F. Matthews, M. Mayer, P. Petersson, M. Rubel, W. van Renterghem, I. Uytdenhouwen, JET-EFDA Contributors, Global erosion and deposition patterns in JET with the ITER-like wall, J. Nucl. Mater. 463 (2015) 157–161. doi:10.1016/j.jnucmat.2015.01.038.

[11] A. Widdowson, E. Alves, A. Baron-Wiechec, N.P. Barradas, N. Catarino, J.P. Coad, V. Corregidor, A. Garcia-Carrasco, K. Heinola, S. Koivuranta, S. Krat, A. Lahtinen, J. Likonen, M. Mayer, P. Petersson, M. Rubel, S. Van Boxel, Overview of the JET ITER-like wall divertor, Nucl. Mater. Energy. 12 (2017) 499–505. doi:10.1016/j.nme.2016.12.008.

[12] A. Widdowson, E. Alves, C.F. Ayres, A. Baron-Wiechec, S. Brezinsek, N. Catarino, J.P. Coad, K. Heinola, J. Likonen, G.F. Matthews, M. Mayer, M. Rubel, JET-EFDA

Contributors, Material migration patterns and overview of first surface analysis of the JET ITER-like wall, Phys. Scr. T159 (2014) 014010. doi:10.1088/0031-8949/2014/T159/014010.

[13] A. Widdowson, J.P. Coad, E. Alves, A. Baron-Wiechec, N.P. Barradas, N. Catarino, V. Corregidor, K. Heinola, S. Krat, J. Likonen, G.F. Matthews, M. Mayer, P. Petersson, M. Rubel, Impurity re-distribution in the corner regions of the JET divertor, Phys. Scr. T170 (2017) 014060. doi:10.1088/1402-4896/aa90d5.

[14] M. Mayer, S. Krat, A. Baron-Wiechec, Y. Gasparyan, K. Heinola, S. Koivuranta, J. Likonen, C. Ruset, G. De Saint-Aubin, A. Widdowson, JET Contributors, Erosion and deposition in the JET divertor during the second ITER-like wall campaign, Phys. Scr. (2017) 014058. doi:10.1088/1402-4896/aa8ff9.

[15] N. Catarino, N.P. Barradas, V. Corregidor, A. Widdowson, A. Baron-Wiechec, J.P. Coad, K. Heinola, M. Rubel, E. Alves, Assessment of erosion, deposition and fuel retention in the JET-ILW divertor from ion beam analysis data, Nucl. Mater. Energy. 12 (2017) 559–563. doi:10.1016/j.nme.2016.10.027.

[16] A. Widdowson, J.P. Coad, E. Alves, A. Baron-Wiechec, N.P. Barradas, S. Brezinsek, N. Catarino, V. Corregidor, K. Heinola, S. Koivuranta, S. Krat, A. Lahtinen, J. Likonen, G.F. Matthews, M. Mayer, P. Petersson, M. Rubel, J. Contributors, Overview of fuel inventory in JET with the ITER-like wall, Nucl. Fusion. 57 (2017) 086045. doi:10.1088/1741-4326/aa7475.

[17] Sunwoo Moon, P. Petersson, M. Rubel, E. Fortuna-Zalesna, A. Widdowson, S. Jachmich, A. Baron-Wiechec, A. Litnovsky, E. Alves, J. Contributors, First Mirror Test in JET for ITER: complete overview after three ILW campaigns, Submitted to Nucl. Mater. Energy. (2018).

[18] J.P. Coad, H.-G. Esser, J. Likonen, M. Mayer, G. Neill, V. Philipps, M. Rubel, J.

Vince, JET-EFDA Contributors, Diagnostics for studying deposition and erosion processes in JET, Fusion Eng. Des. 74 (2005) 745–749. doi:10.1016/j.fusengdes.2005.06.217.

[19] P. Strom, Petersson, M. Rubel, E. Fortuna-Zalesna, A. Widdowson, G. Sergienko, J. Contributors, Co-deposition of deuterium and impurity atoms on wall probes in the divertor of JET with ITER-like wall, Submitted to Nucl. Mater. Energy. (2018).

[20] A. Widdowson, J.P. Coad, E. Alves, A. Baron-Wiechec, N.P. Barradas, N. Catarino, V. Corregidor, K. Heinola, S. Krat, J. Likonen, G.F. Matthews, M. Mayer, P. Petersson, M. Rubel, JET Contributors, Impurity re-distribution in the corner regions of the JET divertor, Phys. Scr. T170 (2017) 014060. doi:10.1088/1402-4896/aa90d5.

[21] A. Kirschner, S. Brezinsek, A. Huber, A. Meigs, G. Sergienko, D. Tskhakaya, D. Borodin, M. Groth, J. Romazanov, S. Wiesen, C. Linsmeier, J. Contributors, Modelling of tungsten erosion and deposition in the divertor of JET-ILW in comparison to expeimental findings, Submitted to Nucl. Mater. Energy. (2018).

[22] J.P. Coad, J. Likonen, M. Rubel, E. Vainonen-Ahlgren, D.E. Hole, T. Sajavaara, T. Renvall, G.F. Matthews, JET EFDA Contributors, Overview of material re-deposition and fuel retention studies at JET with the Gas Box divertor, Nucl. Fusion. 46 (2006) 350–366. doi:10.1088/0029-5515/46/2/018.

[23] V. Bobkov, D. Aguiam, R. Bilato, S. Brezinsek, L. Colas, A. Czarnecka, P. Dumortier, R. Dux, H. Faugel, H. Fünfgelder, P. Jacquet, A. Kallenbach, A. Krivska, C.C. Klepper, E. Lerche, Y. Lin, D. Milanesio, R. Maggiora, I. Monakhov, R. Neu, J.-M. Noterdaeme, R. Ochoukov, T. Pütterich, M. Reinke, W. Tierens, A. Tuccilo, O. Tudisco, D. Van Eester, J. Wright, S. Wukitch, W. Zhang, the A.U. Team, Team, A. C-Mod, Team, Euro.M. Team, JET Contributors, Impact of ICRF on the scrape-off layer and on plasma wall interactions: from present experiments to fusion reactor, 23rd

Conf. Plasma Surf. Interact. (2018).

[24] M. Mayer, S. Krat, J.P. Coad, A. Hakola, J. Likonen, S. Lindig, A. Widdowson, JET-EFDA Contributors, Erosion at the inner wall of JET during the discharge campaigns 2001–2009, J. Nucl. Mater. 438 (2013) S780–S783. doi:10.1016/j.jnucmat.2013.01.167.

[25] M. Schmid, Sputter Yield Calculator, (2009). https://www.iap.tuwien.ac.at/www/surface/sputteryield.

[26] N. Matsunami, Y. Yamamura, Y. Itikawa, N. Itoh, Y. Kazumata, S. Miyagawa, K. Morita, R. Shimizu, H. Tawara, Energy dependence of the ion-induced sputtering yields of monatomic solids, Atomic Data Nucl. Data Tables. 31 (1984) 1–80. doi:10.1016/0092-640X(84)90016-0.

[27] M. Sertoli, J.C. Flanagan, M. Bacharis, O. Kardaun, A. Jarvinen, G.F. Matthews, S. Brezinsek, D. Harting, A. Cackett, E. Hodille, I.H. Coffey, E. Lazzaro, T. Pütterich, JET-EFDA contributors, Impact of W events and dust on JET-ILW operation, J. Nucl. Mater. 463 (2015) 837–841. doi:10.1016/j.jnucmat.2014.12.033.

[28] M. Rubel, A. Widdowson, J. Grzonka, E. Fortuna-Zalesna, S. Moon, P. Petersson, N. Ashikawa, N. Asakura, D. Hamaguchi, Y. Hatano, K. Isobe, S. Masuzaki, H. Kurotaki, Y. Oya, M. Oyaidzu, M. Tokitani, Dust generation in tokamaks: Overview of beryllium and tungsten dust characterisation in JET with the ITER-like wall, Fusion Eng. Des. (2018). doi:10.1016/j.fusengdes.2018.03.027.

7. Figure Captions

Figure 1: Nickel concentrations across a Tile 1 exposed for each of ILW1, ILW2 and ILW3. Inset: cross-section of Tile 1 showing the s-coordinates along its surface.

Figure 2. Tungsten concentration on a louvre clip at the outer divertor corner exposed in ILW2.

Figure 3. (a) Nickel, chromium and iron concentrations on IWGL tile 2XR10 after ILW3. (b) Transmission electron micrograph and elemental analysis showing layered deposit containing chromium from ILW1 Be limiter tile.

Figure 4. Tungsten concentration on 2XR10 after each ILW campaign.

Figure 5: Tungsten concentration on the WPL tile 4D14 after ILW1 and ILW2

Figure 6: Transient impurity events for ILW1, ILW2 and ILW3 for (a) tungsten and (b) nickel, chromium iron particles. For each bar the number of TIEs for the given element(s) and total number of TIEs per 500 pulse bin width are shown.

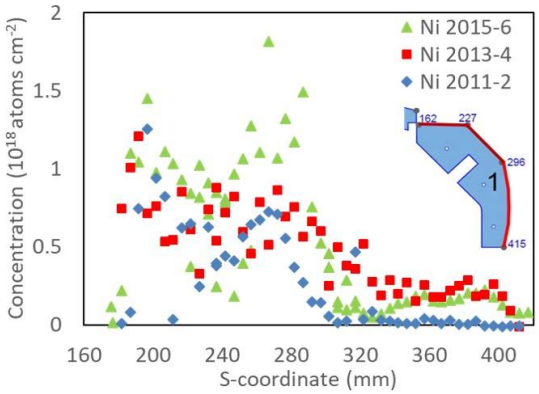

Figure 1: Nickel concentrations across a Tile 1 exposed for each of ILW1, ILW2 and ILW3. Inset: cross-section of Tile 1 showing the s-coordinates along its surface.

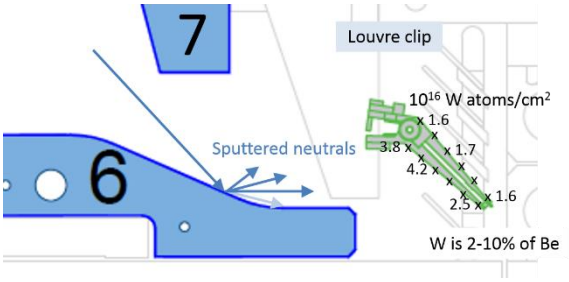

Figure 2. Tungsten concentration on a louvre clip at the outer divertor corner exposed in ILW2.

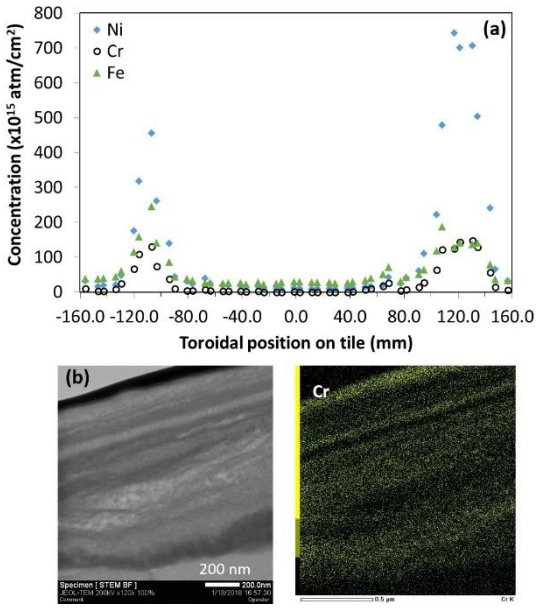

Figure 3. (a) Nickel, chromium and iron concentrations on IWGL tile 2XR10 after ILW3. (b) Transmission electron micrograph and elemental analysis showing layered deposit containing chromium from ILW1 Be limiter tile.

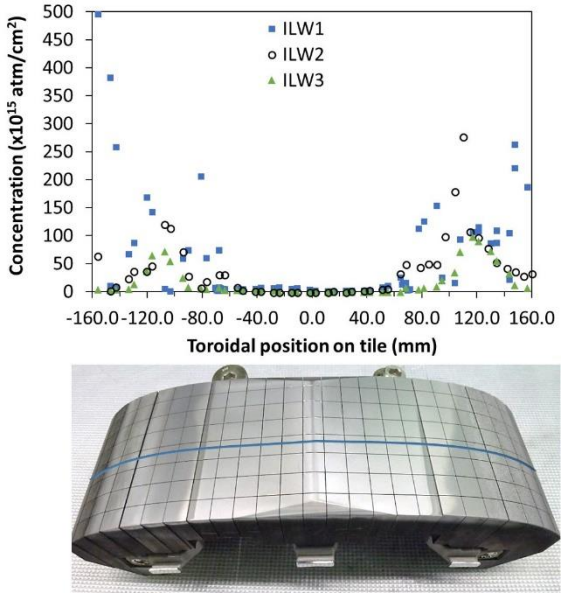

Figure 4. Tungsten concentration on 2XR10 after each ILW campaign.

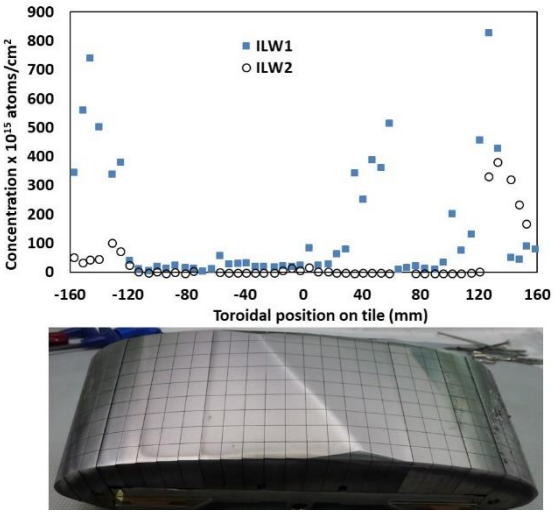

Figure 5: Tungsten concentration on the WPL tile 4D14 after ILW1 and ILW2.

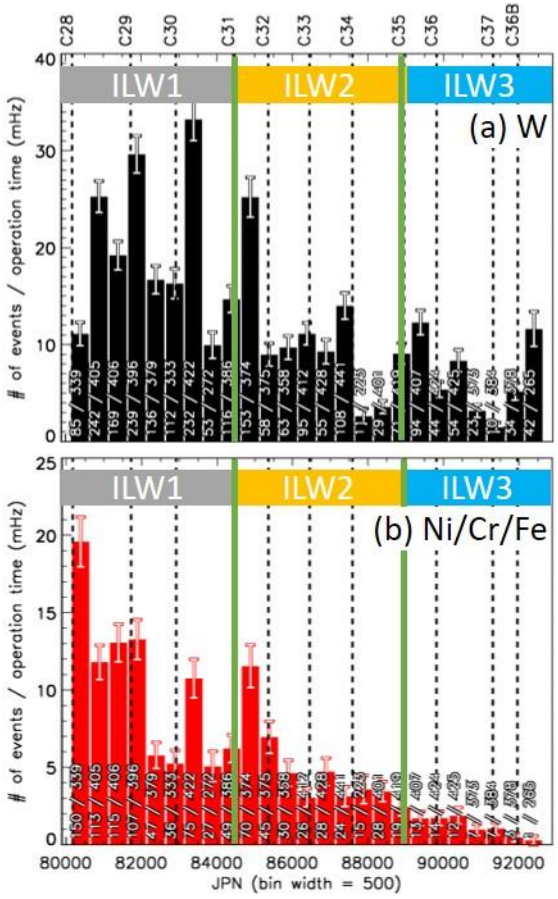

Figure 6: Transient impurity events for ILW1, ILW2 and ILW3 for (a) tungsten and (b) nickel, chromium iron particles. For each bar the number of TIEs for the given element(s) and total number of TIEs per 500 pulse bin width are shown.